12-1-2005

Glycosylphosphatidylinositol-anchored proteins are required for cell wall synthesis and morphogenesis in arabidopsis

C. Stewart Gillmor
Carnegie Institution of Washington

Wolfgang Lukowitz
Carnegie Institution of Washington

Ginger Brininstool
Carnegie Institution of Washington

John C. Sedbrook
Carnegie Institution of Washington

Thorsten Hamann
Carnegie Institution of Washington

See next page for additional authors

Recommended Citation

Stewart Gillmor, C., Lukowitz, W., Brininstool, G., Sedbrook, J., Hamann, T., Poindexter, P., & Somerville, C. (2005). Glycosylphosphatidylinositol-anchored proteins are required for cell wall synthesis and morphogenesis in arabidopsis. *Plant Cell, 17* (4), 1128-1140. https://doi.org/10.1105/tpc.105.031815

The Plant Cell, Vol. 17, 1128–1140, April 2005, www.plantcell.org

Glycosylphosphatidylinositol-Anchored Proteins Are Required for Cell Wall Synthesis and Morphogenesis in Arabidopsis

C. Stewart Gillmor,[a,b,1] Wolfgang Lukowitz,[a,2] Ginger Brininstool,[a] John C. Sedbrook,[a,3] Thorsten Hamann,[a] Patricia Poindexter,[a] and Chris Somerville[a,b,4]

[a] Department of Plant Biology, Carnegie Institution, Stanford, California 94305
[b] Department of Biological Sciences, Stanford University, Stanford, California 94305

Mutations at five loci named *PEANUT1-5* (*PNT*) were identified in a genetic screen for radially swollen embryo mutants. *pnt1* cell walls showed decreased crystalline cellulose, increased pectins, and irregular and ectopic deposition of pectins, xyloglucans, and callose. Furthermore, *pnt1* pollen is less viable than the wild type, and *pnt1* embryos were delayed in morphogenesis and showed defects in shoot and root meristems. The *PNT1* gene encodes the *Arabidopsis thaliana* homolog of mammalian PIG-M, an endoplasmic reticulum–localized mannosyltransferase that is required for synthesis of the glycosylphosphatidylinositol (GPI) anchor. All five *pnt* mutants showed strongly reduced accumulation of GPI-anchored proteins, suggesting that they all have defects in GPI anchor synthesis. Although the mutants are seedling lethal, *pnt1* cells are able to proliferate for a limited time as undifferentiated callus and do not show the massive deposition of ectopic cell wall material seen in *pnt1* embryos. The different phenotype of *pnt1* cells in embryos and callus suggest a differential requirement for GPI-anchored proteins in cell wall synthesis in these two tissues and points to the importance of GPI anchoring in coordinated multicellular growth.

INTRODUCTION

The plant extracellular matrix is composed of polysaccharides, proteins, and glycoproteins and plays a crucial role in morphogenesis and development of plants. The synthesis and organization of cellulose and xyloglucan polymers largely determines the mechanical characteristics of the wall, and the pectin network is crucial for cell adhesion and wall porosity. Cellulose microfibrils are synthesized by plasma membrane enzyme complexes and are extruded directly into the cell wall (reviewed in Williamson et al., 2002). By contrast, the other polysaccharides and proteins of the cell wall are synthesized in the endoplasmic reticulum (ER) or Golgi and reach the cell wall through the secretory pathway (Gibeaut and Carpita, 1994). The mechanisms by which these polymers are assembled into functional networks are unknown.

Many proteins found in the cell wall are posttranslationally modified. The importance of *N*-glycosylation for cellulose biosynthesis has been demonstrated (Lukowitz et al., 2001; Burn et al., 2002; Gillmor et al., 2002). Another posttranslational modification of cell wall–localized proteins is the addition of a glycosylphosphatidylinositol (GPI) membrane anchor, which is synthesized by enzyme complexes associated with the ER membrane. Proteins to be modified with a GPI anchor are cotranslationally inserted into the ER and typically contain a single C-terminal transmembrane domain that is proteolytically cleaved during transfer of the protein to the GPI anchor (Kinoshita and Inoue, 2000). The final destination of GPI-anchored proteins is the plasma membrane, where the anchor allows hydrophilic polypeptides to stably associate with the extracellular face of the membrane. The GPI moiety can be cleaved by specific phospholipases, releasing the polypeptide into the extracellular matrix in a regulated manner. In addition, evidence exists for the association of GPI-anchored proteins into lipid rafts, higher order structures that can coordinate enzymatic functions or signaling events (Ferguson, 1999; Peskan et al., 2000; Borner et al., 2005).

GPI-anchored proteins (GAPs) have been implicated in many processes. The coat of trypanosomes consists of GPI-anchored surface glycoproteins, which serve to make these parasites antigenically variable (Ferguson, 1999). In animals, mutations in a class of GPI-anchored glycoproteins called glypicans cause defects in cell division and tissue morphogenesis (Selleck, 2000). The genome of the yeast *Saccharomyces cerevisiae* encodes for ~50 GAPs, many of which are essential for cell wall synthesis and organization or for cell–cell signaling in the mating response (Caro et al., 1997; Kapteyn et al., 1999). Recent studies have focused on a genome-wide identification of the total set of GAPs in *Arabidopsis thaliana* (Borner et al., 2002, 2003; Eisenhaber et al., 2003). Based on their sequences, the 250 or so predicted GAPs of Arabidopsis most likely participate in cell wall deposition and remodeling, defense responses, and cell signaling. Arabinogalactan proteins (AGPs), a class of heavily glycosylated cell wall proteins, have been the subject of study for several years and are known to be modified by the addition of a GPI anchor

[1] Current address: Department of Biology, University of Pennsylvania, Philadelphia, PA 19104.
[2] Current address: Cold Spring Harbor Laboratory, Cold Spring Harbor, NY 11724.
[3] Current address: Department of Biological Sciences, Illinois State University, Normal, IL 61790.
[4] To whom correspondence should be addressed. E-mail crs@stanford.edu; fax 650-325-6857.
The author responsible for distribution of materials integral to the findings presented in this article in accordance with the policy described in the Instructions for Authors (www.plantcell.org) is: Chris Somerville (crs@stanford.edu).
Article, publication date, and citation information can be found at www.plantcell.org/cgi/doi/10.1105/tpc.105.031815.

(Youl et al., 1998). AGPs are thought to play roles in growth and differentiation, though a mechanism for their action has not been defined (Gaspar et al., 2001).

Only a few predicted or demonstrated GAPs of plants have been functionally characterized. Conditional mutations in the *COBRA* (*COB*) gene were isolated based on their root swelling phenotype, and it was proposed that *COB* is required for oriented cellulose deposition (Schindelman et al., 2001). *BC1*, a homolog of *COB*, is required for normal cellulose levels in secondary cell walls of rice (*Oryza sativa*) plants (Li et al., 2003). Loss of SOS5, a protein with fasciclin and arabinogalactan domains, causes reduced root growth and root swelling (Shi et al., 2003). Mutations in *SKU5* alter the growth properties of roots and affect root waving and cell expansion (Sedbrook et al., 2002). The *PMR6* gene, which encodes a putative pectate lyase, was identified in a genetic screen for mutants with noncompatible interactions with the powdery mildew fungus (*Erysiphe cichoracearum*) (Vogel et al., 2002). The Arabidopsis classical AGP, AGP18, was shown to be required for female gametophyte development (Acosta-García and Vielle-Calzada, 2004). Overexpression of the tomato (*Lycopersicon esculentum*) AGP, LeAGP-1, caused reduced plant growth and seed size (Sun et al., 2004a). Of the above proteins, only SKU5 and LeAGP-1 were experimentally shown to be GPI anchored (Sedbrook et al., 2002; Sun et al., 2004b). A recent article also describes the effect on pollen of loss-of-function mutations in genes of the GPI anchor biosynthesis pathway. *SETH1* and *SETH2* genes were shown to encode homologs of mammalian PIG-C and PIG-A proteins, which are components of the GPI-*N*-acetylglucosaminyltransferase complex. Mutations in *SETH1* and *SETH2* affect pollen germination and growth in vitro and result in abnormal callose deposition in pollen tubes (Lalanne et al., 2004). The above studies all underscore the importance of GAPs for cell wall organization and function.

This work describes mutations in five genes, designated *PEANUT1-5* (*PNT*), required for accumulation of GAPs. The mutants were recovered in a genetic screen for radially swollen embryos (Gillmor et al., 2002). *PNT1* encodes a predicted mannosyltransferase with sequence similarity to human PIG-M, an ER-localized mannosyltransferase that is required for synthesis of the GPI anchor (Maeda et al., 2001). *pnt1* embryos show a large reduction in crystalline cellulose, an increase in pectin, as well as ectopic deposition of xyloglucan, pectin, and callose. Although *pnt1* mutants are embryo lethal, callus differentiated from *pnt1* embryos can grow for a limited time. Ectopic callose deposition is observed in *pnt1* callus, but, in contrast with *pnt1* embryos, cell wall structure appears otherwise normal. Our results highlight the importance of GAPs for the synthesis and secretion of cell wall polymers and point to a reduced requirement for GAPs in the absence of coordinated multicellular development.

RESULTS

pnt Mutants Are Radially Swollen during Embryogenesis

Five *pnt* mutants were recovered by microscopic analysis of embryo and seed morphology (Gillmor et al., 2002). The gene name refers to the characteristic shape and wrinkled seed coat of mutant seeds. Mutant embryos exhibit a radially swollen phenotype that is similar to strong alleles of the cellulose-deficient *rsw1* mutants (Beeckman et al., 2002; Gillmor et al., 2002), in that they show altered polarity of cell expansion in outer cell layers during embryogenesis (Figure 1).

Complementation analysis and mapping demonstrated that the five *pnt* mutants were in five distinct genes, named *PNT1* to *PNT5*. *PNT1* was mapped between the markers T10F18(A) and MWD9(A) and was subsequently identified as gene At5g22130 (see below). *PNT2* was mapped to ~30 centimorgan (cM) on chromosome 5 between the markers nga151 and P01 (in 350 meiotic events, five recombinations between nga151 and *pnt2* and three between *pnt2* and P01 were found). *PNT3* was mapped to ~39 cM on chromosome 1 between the markers F21M12 and ciw12 (in 210 meiotic events, 10 recombinations between F21M12 and *pnt3* and 10 between *pnt3* and ciw12 were found). *PNT4* was mapped to ~45 cM on chromosome 3 between the markers nga162 and ciw4 (in 210 meiotic events, 29 recombinations between nga162 and *pnt4* and 36 between *pnt4* and ciw4 were found). *PNT5* was mapped to ~60 cM on chromosome 4 between the markers g4539 and CH42 (in 240 meiotic events, two recombinations between g4539 and *pnt5* and one between *pnt5* and CH42 were found). All *pnt* mutations were recessive but segregated significantly <25% homozygous mutants upon selfing. Reciprocal crossing experiments with *pnt1* demonstrated that the altered *pnt1* segregation ratio was due to poor transmission through pollen, with no significant effect on egg transmission (Table 1).

Similar to *rsw1-2* (Figure 1B), the root, hypocotyls, and cotyledons of all five classes of *pnt* mutants are swollen. Cells of the outer layers of the embryonic root and hypocotyl are brick shaped (Figures 1C to 1G), as opposed to the typical cube-shaped epidermal and endodermal cells of wild-type embryos (Figure 1A, magnification of the root in Figure 1H). Unlike mutations in *rsw1*, which primarily cause defects in cell elongation, *pnt* mutations also cause developmental defects. The shoot apical meristem of *pnt* embryos is greatly enlarged compared with that of the wild type (Figure 1I). As seen in Figure 1D (arrowheads), *pnt* mutants commonly have three or four cotyledons, compared with two cotyledons in wild-type embryos (Figure 1A). Furthermore, *pnt* embryos lack most cells of the root cap, and the cells of the quiescent center and initials of the endodermis are disorganized (Figure 1H). Because of the similarity of all five *pnt* mutants, we chose to characterize the *pnt* phenotype by studying *pnt1* in detail.

Delayed Morphogenesis and Abnormal Cell Divisions in *pnt1* Embryos

The appearance of cotyledons during the progression from the globular to heart stage of embryo development constitutes a transition from radial to bilateral symmetry (cf. Figures 2A and 2C). *pnt1* embryos are consistently delayed in this transition. Compared with the wild-type heart stage embryo in Figure 2C, the *pnt1* embryo shown in Figure 2D remains radially symmetrical, although it has increased considerably in size compared with the globular stage *pnt1* embryo shown in Figure 2B. Later in

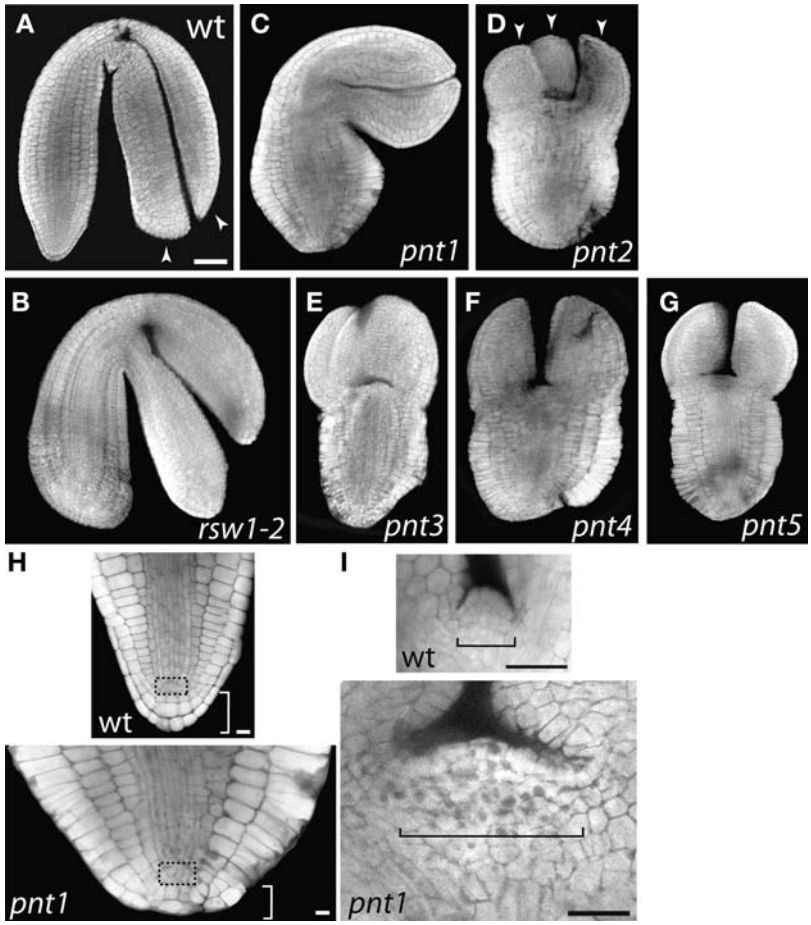

Figure 1. *pnt* Mutants Are Radially Swollen.

Confocal images of the wild type **(A)**, *rsw1-2* **(B)**, *pnt1* **(C)**, *pnt2* **(D)**, *pnt3* **(E)**, *pnt4* **(F)**, and *pnt5* **(G)** at the late bent cotyledon stage of embryogenesis. Confocal sections of the wild type and *pnt1* root **(H)** and shoot **(I)** meristems of dissected late bent cotyledon stage embryos. **(A)** to **(G)** are shown at the same magnification. Arrowheads in **(A)** and **(D)** point to cotyledons. Root meristem region is boxed in **(H)**; shoot meristem region is indicated with a bracket in **(I)**. Bars = 50 μm in **(A)** and 25 μm in **(H)** and **(I)**.

development at the torpedo stage, two classes of *pnt1* embryos are apparent: those that have made the transition to bilateral symmetry by developing two cotyledons (Figure 2F) and those that have increased in size, but which remain radially symmetrical (Figure 2G). A comparison of the percentage of *pnt1* embryos with delayed morphogenesis at the torpedo stage and the number of late bent cotyledon stage *pnt1* embryos with three or more cotyledons is shown in Figure 2H. At the torpedo stage of development, 32% of *pnt1* embryos have developed cotyledon primordia, whereas 68% remain round ($n = 174$). At the late bent cotyledon stage of development, 34% of *pnt1* embryos have two cotyledons, whereas 66% have three or more cotyledons ($n = 210$). Thus, there is a good correlation between a delay in the initiation of cotyledon primordia and the development of extra cotyledons (see also Torres-Ruíz and Jürgens, 1994).

In addition to delaying morphogenesis, *pnt1* mutations also interfere with the normal pattern of cell division in the early embryo. For example, the globular stage *pnt1* embryo shown in Figure 2B has several irregular oblique divisions in the proembryo (arrowhead), and the hypophysis, the cell supporting the proembryo, remains undivided. This is in contrast with corresponding wild-type embryos (Figure 2A), where the hypophysis divides to produce a lens-shaped derivative that will form the quiescent center of the root meristem and a basal derivative that forms the central root cap (Jürgens and Mayer, 1994). By the heart stage, the *pnt1* embryo shown in Figure 2D has produced a cell similar in size and shape to a wild-type lens cell, but the basal derivative of the hypophysis is unusually large and has an irregular shape. Furthermore, continued oblique divisions in the proembryo make it difficult to distinguish elongated vascular precursor cells (visible in the wild type, Figure 2C). Thus, the anatomical defects observed in the root meristem and root cap of late-stage *pnt1* embryos (Figure 1H) are correlated with abnormal cell divisions of the hypophyseal cell and its derivatives during early embryogenesis.

Table 1. Reduced Transmission of the *pnt1-1* Allele through Pollen

Cross (Male × Female)	*pnt1/pnt1* or *pnt1/PNT1* Segregation in F1[a]	
	Observed	Expected[b]
pnt1/PNT1 × *pnt1/PNT1* (selfed)	2.7% Top half silique	12.5% Top half silique
	2.6% Bottom half silique	12.5% Bottom half silique
	5.3% Total *pnt1/pnt1* ($n = 1132$)	25% Total *pnt1/pnt1*
pnt1/PNT1 × *PNT1/PNT1*	7% *pnt1/PNT1* ($n = 100$)	50% *pnt1/PNT1*
PNT1/PNT1 × *pnt1/PNT1*	46.3% *pnt1/PNT1* ($n = 108$)	50% *pnt1/PNT1*

[a] For the *pnt1/PNT1* × *pnt1/PNT1* cross, F1 progeny were scored directly by counting mutant embryos in the upper and lower halves of the silique. For *pnt1/PNT1* × *PNT1/PNT1* and *PNT1/PNT1* × *pnt1/PNT1* crosses, the genotype of F1 plants was ascertained by scoring the segregation of F2 mutant embryos in the siliques of selfed F1 plants.

[b] Expected segregation for a recessive nuclear gene with normal transmission.

Seedling-Lethal *pnt1* Mutants Are Able to Proliferate as Callus

A wild-type Arabidopsis seedling grown for 5 d on tissue culture medium is shown in Figure 3A. By this stage, the cotyledons have expanded, the first true leaves are apparent, and the root system has begun to develop. By contrast, *pnt1* seedlings of similar age show little sign of postembryonic development (Figure 3B). After seed imbibition, *pnt1* embryos expand slightly and emerge from the seed coat (cf. with *pnt1* seed shown in Figure 3C) but soon become necrotic. In contrast with the lethality of *pnt1* seedlings, when green late-stage *pnt1* embryos were dissected out of the ovule and placed on callus-inducing media, *pnt1* calli (Figure 3E) were able to grow for 4 to 6 weeks, with a growth rate similar to calli from wild-type embryos (Figure 3D), before undergoing necrosis (dark brown tissue in Figure 3E). This result suggests that the undifferentiated growth typical of callus tissue is more permissive for loss of the *PNT1* gene product than the coordinated multicellular growth required for seedling development.

Decreased Cellulose, Increased Pectin, and Neutral Sugars in *pnt1* Embryos

The phenotypic similarity of *pnt1* and *rsw1-2* phenotypes during embryogenesis suggested that *pnt1* mutants might also have cell wall alterations. To test this hypothesis, we quantified the sugar composition of cell wall polysaccharides in late bent cotyledon

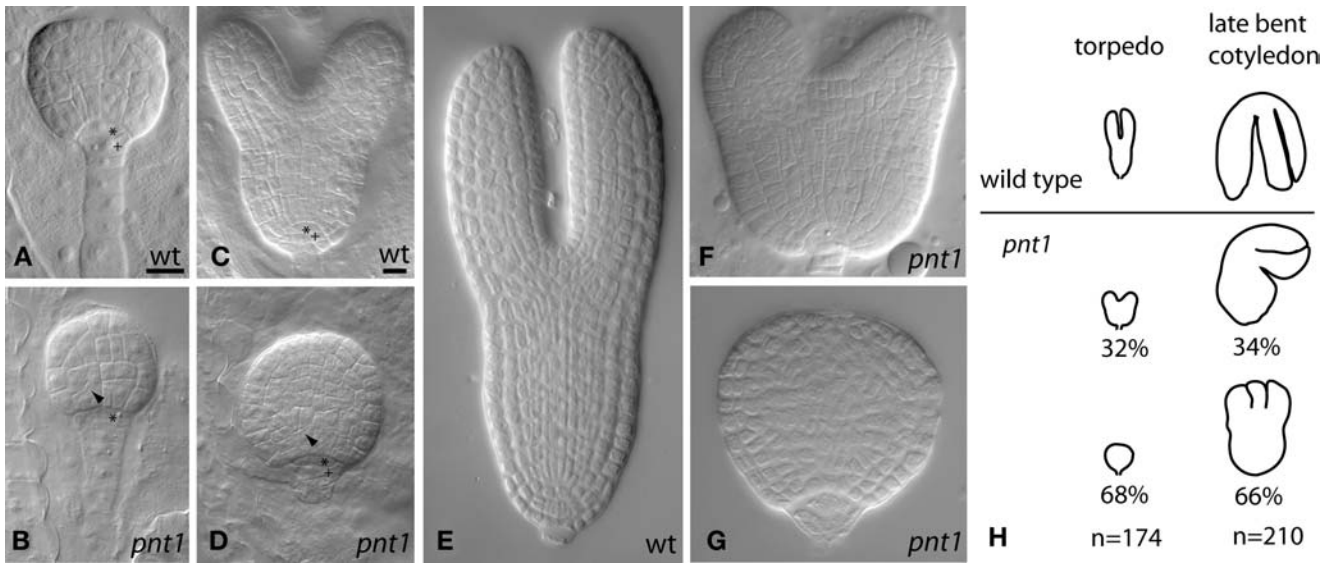

Figure 2. Delayed Morphogenesis and Abnormal Cell Divisions in *pnt1* Embryos.

(A) to **(G)** Wild type (**[A]**, **[C]**, and **[E]**) and *pnt1* (**[B]**, **[D]**, **[F]**, and **[G]**) embryos shown at the late globular (**[A]** and **[B]**), late heart (**[C]** and **[D]**), and torpedo (**[E]** to **[G]**) stages of embryogenesis. Embryos within ovules (**[A]** to **[D]**) and dissected embryos (**[E]** to **[G]**) were cleared in Hoyer's solution and viewed with Nomarski optics. Arrowheads, oblique cell division; asterisk, apical daughter of hypophyseal cell; cross, basal daughter of hypophyseal cell. Bars = 10 μm. **(A)** and **(B)** are the same magnification. **(C)** to **(G)** are the same magnification.

(H) Tracings of typical wild-type and *pnt1* embryos at the wild-type torpedo (left) and late bent cotyledon (right) stages. The percentage of *pnt1* embryos with bilateral (top) or radial (bottom) symmetry at the wild-type torpedo stage is shown at the left. The percentage of *pnt1* embryos with two cotyledons (top) or three or more cotyledons (bottom) at the late bent cotyledon stage is shown at the right.

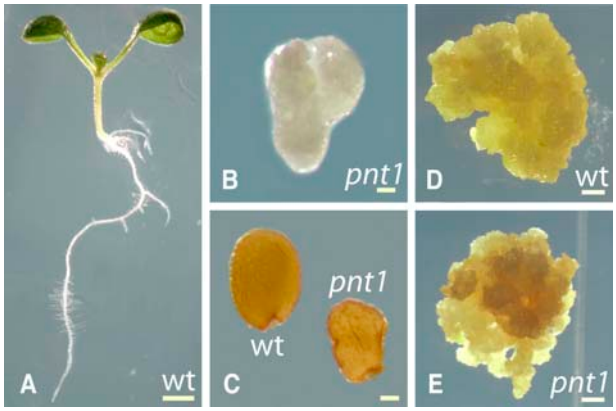

Figure 3. *pnt1* Mutants Are Seedling Lethal, but *pnt1* Callus Is Able to Proliferate.

Bright-field images of wild-type **(A)** and *pnt1* **(B)** seedlings after 5 d of growth on solidified agar medium plus sucrose. Mature wild-type and *pnt1* seeds are shown in **(C)**. Six-week-old callus induced from wild-type **(D)** and *pnt1* **(E)** late stage immature embryos. Bars = 1 mm in **(A)**, 100 μm in **(B)** and **(C)**, and 1 mm **(D)** and **(E)**.

stage wild-type and *pnt1* embryos. The results of these analyses are shown in Table 2. *pnt1* embryos had a 40% reduction in crystalline cellulose (117 nmol glucose/mg dry weight) compared with 196 nmol/mg in wild-type embryos. By contrast, *pnt1* embryos contained 93 nmol/mg dry weight of uronic acid (the principal component of pectin), more than twice as much as wild-type embryos (41 nmol/mg). Other noncellulosic polymers were quantified by measuring their neutral sugar constituents. Wild-type embryos had 483 nmol total neutral sugars/mg dry weight, whereas *pnt1* embryos were found to have 782 nmol/mg dry weight, a 60% increase. Although the total amount of neutral sugars differed between wild-type and *pnt1* embryos, the ratio of the amounts of the different neutral sugars did not vary significantly (Table 2).

Chemical analysis of *pnt1* cell walls illustrated that, although *pnt1* and *rsw1-2* have similar radially swollen phenotypes, the two mutants have significantly different cell wall compositions. The primary effect of the *rsw1-2* mutation was a 75% reduction in crystalline cellulose, concomitant with a slight, possibly compensatory, increase in pectin (Gillmor et al., 2002). Whereas the cellulose decrease in *pnt1* embryos (40%) is less dramatic than that of *rsw1-2*, the *pnt1* mutation has a much greater effect on the other polysaccharide constituents of the wall.

Ectopic Accumulation of Xyloglucan, Pectin, and Callose in *pnt1* Embryos and Ectopic Callose in *pnt1* Callus

The increased amount of uronic acid and neutral sugars measured in *pnt1* embryos suggested that the distribution or deposition of noncellulosic structural polysaccharides might also be altered. Reagents that specifically identify various polysaccharides were used to determine the spatial distribution of xyloglucan, pectin, and callose in wild-type and *pnt1* embryos. The CCRC M1 antibody recognizes a terminal α-(1,2)-linked fucosyl residue present on xyloglucans (Puhlmann et al., 1994). As shown in Figure 4A, CCRC M1 recognizes epitopes throughout the wild-type cell wall, with the exception of triangular areas at cell junctions. CCRC M1 epitopes are also present throughout *pnt1* embryos, though staining is more diffuse than in the wild type (Figure 4B). In addition, ectopic patches of signal are seen in many cells. The monoclonal antibody JIM5 recognizes esterified pectins (Knox et al., 1990). In sections of wild-type embryos, the strongest JIM5 signal is seen in a triangular area at three cell junctions. JIM5 signal is also seen at lower intensity in a thin line corresponding to the middle lamella between adjacent cell walls (Figure 4C). In *pnt1* embryos, JIM5 epitopes are more abundant than in the wild type and are not confined to the middle lamella and three cell junctions (Figure 4D). Ectopic patches of JIM5 staining, similar to the patches seen with the CCRC M1 antibody, are frequent.

The abnormal chemical composition of *pnt1* cell walls, and the aberrant localization of pectin and xyloglucan epitopes, suggested that the mechanical integrity of *pnt1* cell walls might be compromised. Production of the 1,3-β-glucan, callose, is a common stress response and has been observed in the cellulose-deficient mutant *cyt1* (Nickle and Meinke, 1998; Lukowitz et al., 2001). Callose is synthesized in pollen tubes and transiently during cell wall formation but is not normally found in most plant cell walls (Delmer, 1987). Thus, ectopic callose deposition can be interpreted as a marker of compromised cell wall integrity. Sirofluor, a fluorophore that specifically binds callose (Stone et al., 1984), was used to determine if *pnt1* embryos accumulate callose during embryogenesis. As shown in Figure 4E, late bent cotyledon stage wild-type embryos have no appreciable sirofluor staining. This is in marked contrast with the ectopic accumulation of callose throughout the *pnt1* embryo shown in Figure 4F. At higher magnification (Figure 4H), callose staining is seen in a punctate pattern throughout *pnt1* cell walls, as well as in large patches.

Table 2. Cell Wall Composition of Wild-Type and *pnt1* Embryos[a]

Cell Wall Component	Wild Type		*pnt1*	
Cellulose[b]	196 ± 17		117 ± 11	
Pectin[c]	41 ± 3		93 ± 4	
Neutral sugars[d]				
Rhamnose	35 ± 3	(7%)	62 ± 2	(8%)
Fucose	18 ± 2	(4%)	20 ± 1	(3%)
Arabinose	248 ± 29	(51%)	416 ± 17	(53%)
Xylose	104 ± 13	(22%)	139 ± 4	(18%)
Mannose	18 ± 5	(4%)	16 ± 2	(2%)
Galactose	60 ± 6	(12%)	129 ± 10	(16%)
Total nmol neutral sugars	483		782	
Average dry weight per embryo	4.8 μg		3 μg	

[a] Expressed as nmol sugar/mg dry weight of embryo. Value is the average of at least three measurements, with standard deviation.
[b] Cellulose measured as acetic/nitric acid–insoluble glucose.
[c] Pectin measured as total uronic acid after trifluoroacetic acid hydrolysis.
[d] Amount of each neutral sugar as a percentage of the total neutral sugars is listed in parentheses.

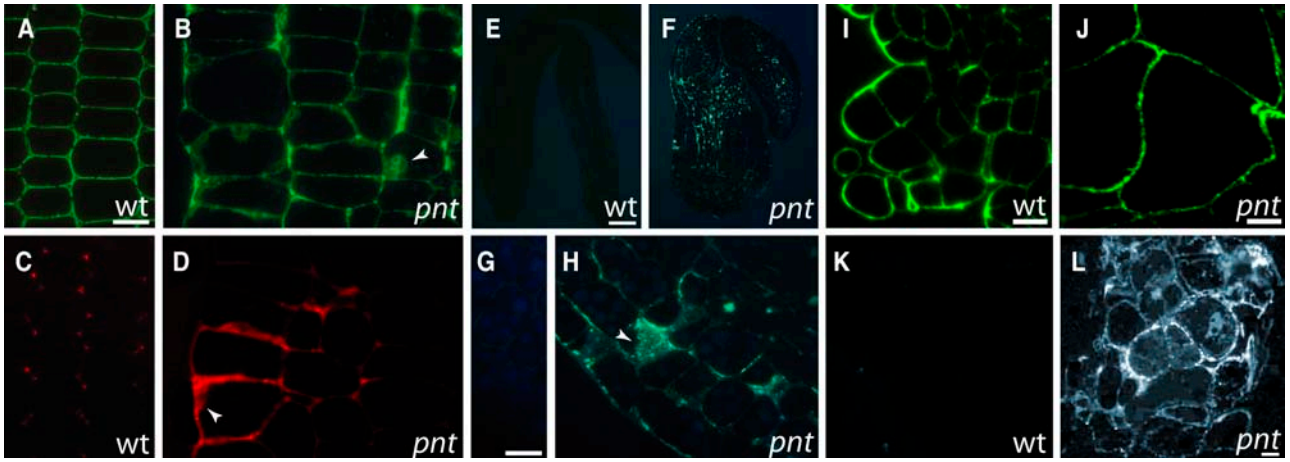

Figure 4. Ectopic Deposition of Xyloglucan, Pectin, and Callose in *pnt1* Embryos and Callose Deposition in *pnt1* Callus.

Sections of wild-type (**[A]**, **[C]**, **[E]**, and **[G]**) and *pnt1* (**[B]**, **[D]**, **[F]**, and **[H]**) embryos at the late bent cotyledon stage of development. Sections of 2-week-old callus differentiated from wild-type (**[I]** and **[K]**) and *pnt1* (**[J]** and **[L]**) seeds. Sections in **(A)**, **(B)**, **(I)**, and **(J)** were incubated with the CCRC-M1 antibody, which recognizes terminal α-(1,3)-linked fucose residues on xyloglucans (Puhlmann et al., 1994). Sections in **(C)** and **(D)** were incubated with JIM5 antibody, which recognizes esterified pectins (Knox et al., 1990). Sections in **(E)** to **(H)** were stained with the callose-specific analine blue fluorochrome Sirofluor, which fluoresces yellow-white when bound to callose. Sections in **(K)** and **(L)** were incubated with anti-β-1,3 glucan antibody. Arrowheads in **(B)**, **(D)**, and **(H)** indicate ectopic patches of signal. Bars = 5 μm in **(A)** and **(G)**, 50 μm in **(E)**, and 10 μm **(I)** and **(L)**. **(A)** to **(D)**, **(G)** and **(H)**, **(E)** and **(F)**, **(I)** and **(J)**, and **(K)** and **(L)** are shown at equal magnification.

We also examined the cell wall phenotype of wild-type and *pnt1* callus cells. Staining of wild-type and *pnt1* callus with CCRC M1 showed that both exhibit a similar pattern of fluorescence associated with xyloglucan in the cell walls (Figures 4I and 4J). Interestingly, *pnt1* callus cells lack the patches of ectopic xyloglucan epitope seen in *pnt1* embryo cells. We used a 1,3-β-glucan antibody to visualize callose deposition in wild-type and *pnt1* calli. No staining was detected in wild-type callus cells (Figure 4K), whereas abundant signal was detected in the *pnt1* callus (Figure 4L). The abundance of callose in *pnt1* callus is consistent with the frequent occurrence of cell death in *pnt1* callus (Figure 3E; data not shown).

Our light microscopic analysis revealed that the deposition pattern of cell wall polymers was aberrant in *pnt1* embryos. To determine the consequences of these abnormalities for the structural organization of *pnt1* cell walls, ultrathin sections of wild-type and *pnt1* embryos and callus were examined by transmission electron microscopy. Wild-type embryo cell walls have a uniform thickness and appearance. The thin band of electron-dense staining of the middle lamella seen in between adjacent wild-type walls is characteristic of pectic polysaccharides, whereas the electron-translucent areas of the wall are composed mainly of cellulose and xyloglucans (Figures 5A, 5C, and 5E). As expected from our previous findings, *pnt1* embryo cells produce and secrete larger amounts of cell wall material. Two types of wall ultrastructure predominate. The first is an altered primary wall (Figure 5B). This primary wall conserves some elements of wild-type wall structure, with a concentration of electron-dense, presumably pectic material in the center of the wall. However, fibrillar electron-dense material as well as thick electron-dense inclusions and swirls are distributed throughout the wall in an apparently random fashion. In addition, islands of electron-dense material surrounded by a membrane are also observed (hatched box in Figure 5B, enlarged in inset) and point to a secretory defect in *pnt1* mutants. As in the wild type, the contents of these altered primary walls are outside of the cell, on the opposite side of the plasma membrane from the cytoplasm (cf. wild-type cell wall, plasma membrane, and cytoplasm in Figure 5C with *pnt1* in Figure 5D). Accumulation of lipid bodies and protein bodies appeared normal in *pnt1* embryos, and defects in the morphology of cellular organelles were not apparent (data not shown).

The second type of wall structure seen in *pnt1* embryos can best be described as massive, ectopic accumulations of wall material. This material has a heterogeneous appearance and often appears appressed to, but distinct from, the primary wall (arrows in Figure 5F point to junction of primary wall and ectopic wall). Invaginations of cytoplasm are visible within these blobs of wall material (inset, Figure 5F), making it often difficult to determine which parts were topologically outside of the cell and which were in the process of being secreted. Similar to the *pnt1* wall structure seen in Figure 5B, the ectopic wall material contains inclusions of varying electron densities, but fibrillar electron dense material is less commonly observed.

The ultrastructural abnormalities observed in *pnt1* embryo cell walls were, for the most part, not seen in cell walls of *pnt1* callus. As observed by comparing Figures 4I and 4J, *pnt1* callus cells are many times larger than wild-type callus cells. Electron micrographs of wild-type (Figure 5G) and *pnt1* (Figure 5H) callus cells at low magnification show that *pnt1* cells are more highly cytoplasmic than their wild-type counterparts. At higher magnification, *pnt1* callus cell walls are structurally similar to wild-type cell walls, except that they have increased electron-dense staining in the lamella, suggesting increased pectin content,

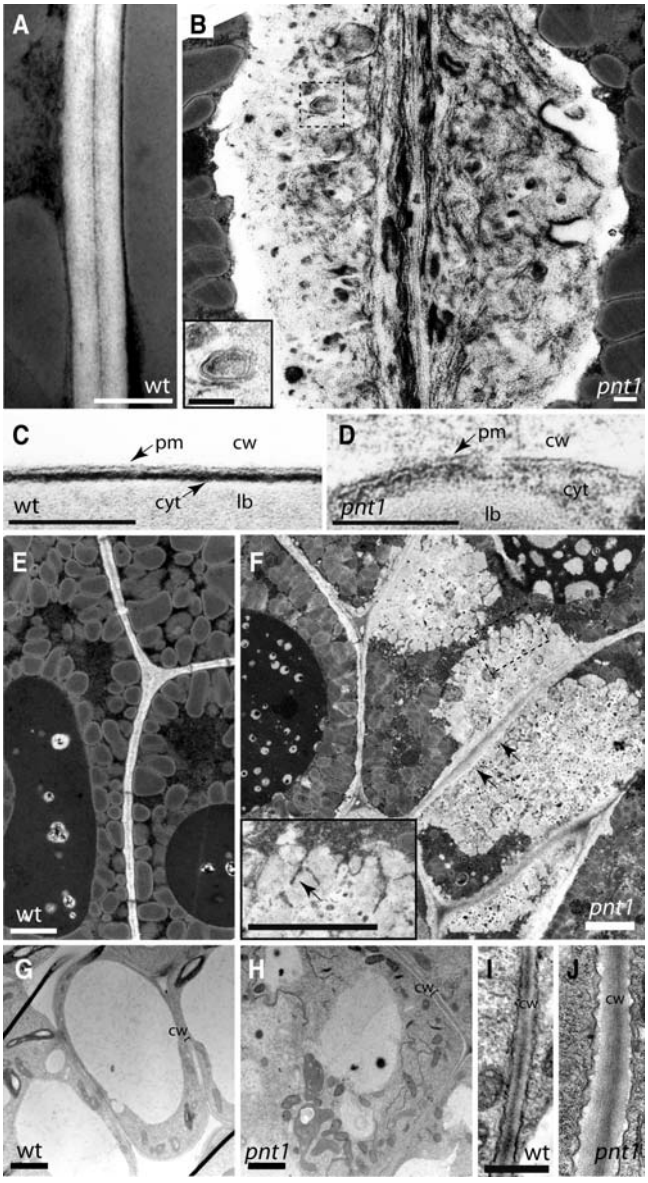

Figure 5. Disorganized and Ectopic Deposition of Cell Wall Material in *pnt1* Embryos and Normal Wall Structure in *pnt1* Callus.

(A) to **(F)** Transmission electron microscopy images of wild-type (**[A]**, **[C]**, and **[E]**) and *pnt1* (**[B]**, **[D]**, and **[F]**) embryo cell walls. *pnt1* **(B)** primary cell walls are disorganized compared with the wild type **(A)**. Inset in **(B)**, electron dense material surrounded by double membrane. Primary cell wall in *pnt1* **(D)** is outside the plasma membrane, as in the wild type **(C)**. *pnt1* cells **(F)** secrete large amounts of ectopic cell wall material that is appressed to more normal primary wall. Inset in **(F)**, cell wall material with blobby morphology. In **(B)** and **(F)**, contents of hatched box are magnified in inset. pm, plasma membrane; cw, cell wall; cyt, cytoplasm; lb, lipid body. Arrowheads in **(F)**, junction of primary and ectopic wall; arrowhead in **(F)** inset, invagination of cytoplasm. Bars = 250 nm in **(A)** and **(B)**, 100 nm in **(C)** and **(D)**, and 2 μm in **(E)** and **(F)**.

(G) to **(J)** Transmission electron microscopy images of cell walls of 2-week-old callus differentiated from wild-type (**[G]** and **[I]**) and *pnt1* (**[H]** and **[J]**) seed. **(I)** and **(J)** are shown at equal magnification. Bars = 2 μm in **(G)** and **(H)** and 500 nm in **(I)**.

and are slightly thicker than wild-type walls. Notably, the ectopic depositions of wall material and drastic alteration in wall structure in *pnt1* embryos were not observed in *pnt1* callus cells (cf. Figure 5B with 5J and Figure 5F with 5H).

In conclusion, *pnt1* embryo cell walls contain increased amounts of cell wall material that are, at least in part, found in large patches appressed to the primary wall. This strongly suggests that *pnt1* mutants are impaired in integrating secreted polysaccharides into a functional wall. It appears as if wall components are initially incorporated into the primary wall in a somewhat disorganized fashion, whereas later the secreted wall material is not integrated into the wall at all, and instead accumulates ectopically. In contrast with *pnt1* embryo cell walls, *pnt1* callus cell walls have an almost normal structure, with only an apparent slight increase in the electron-dense staining characteristic of pectin.

PNT1 Encodes the Arabidopsis Homolog of ER Mannosyltransferase PIG-M

The *PNT1* gene was identified based on its map position and found to correspond to At5g22130 (see Figure 6A for details). The *pnt1-1* allele was found to have a cytosine-to-thymine change at bp 838 of the At5g22130 coding sequence, resulting in a stop at codon 280. The identity of *PNT1* was confirmed by complementation of the *pnt1-1* mutation with a wild-type At5g22130 genomic clone (Figure 6A). A second mutant allele of the *PNT1* gene, *pnt1-2*, was found in the SALK T-DNA insertional line SALK_069393. This second allele, generated in the Columbia ecotype, segregated an embryo mutant with a similar phenotype to *pnt1-1*. The left border of the T-DNA in SALK_069393 was found to be inserted at bp 1051 of the *PNT1* coding sequence. Allelism was confirmed by complementation test. Pollen transmission of the *pnt1-2* allele was slightly increased compared with the *pnt1-1* allele, suggesting that the *pnt1-2* allele may have more enzymatic activity than the ethyl methanesulfonate–induced *pnt1-1* allele. This conclusion is consistent with the fact that the T-DNA insertion in *pnt1-2* occurs downstream of the stop codon in *pnt1-1* (Figure 6A).

Using a *PNT1* cDNA obtained by RT-PCR as a probe, *PNT1* mRNA was found to be present at low levels in roots, hypocotyls, leaves, and stems and at higher levels in the inflorescence meristem (Figure 6B). The predicted PNT1 protein is 38% identical to the human enzyme PIG-M (Figure 6C), an ER membrane–localized 1-4-α-mannosyl transferase that is required for synthesis of the GPI anchor within the ER lumen (Maeda et al., 2001). The *PNT1* gene encodes the only PIG-M homolog in the Arabidopsis genome (data not shown).

GAPs Are Absent in *pnt* Mutants

The similarity of the PNT1 protein to PIG-M suggested that the primary defect of *pnt* mutants was in GPI anchor biosynthesis. To test this hypothesis, we used antibodies against demonstrated and predicted GAPs to test for the presence of these proteins in *pnt* embryos. The SKU5 protein has been shown to be GPI anchored based on the presence of C-terminal consensus sequences and its release from membrane preparations after

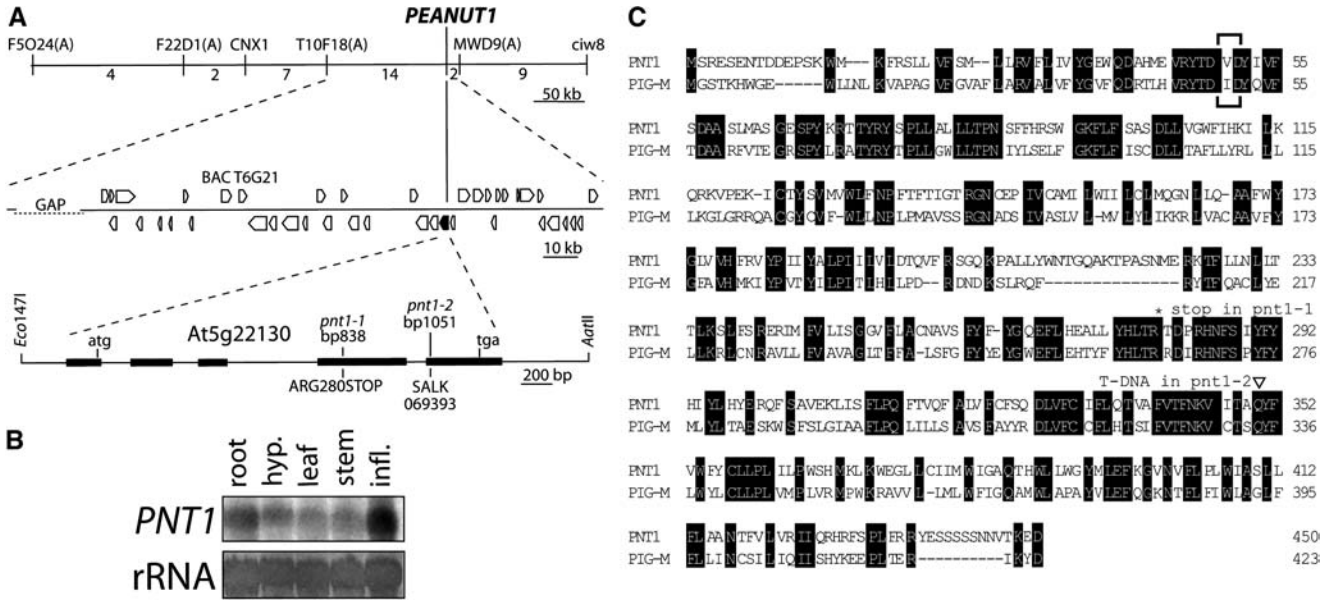

Figure 6. *PNT1* Encodes the Arabidopsis Homolog of PIG-M.

(A) Identification of the *PNT1* gene based on its map position at ~40 cM on chromosome V. Top line, genetic interval used to identify *PNT1*. PCR-based simple sequence length polymorphism markers are shown above the line; the numbers of recombinants recovered between each marker (out of 2010 meiotic products) are shown below the line. Middle line, the ~140-kb physical interval between markers T10F18(A) and MWD9(A), containing 40 predicted genes. Genes are shown as pentagons; *PNT1* is in black. Bottom line, the 3641-bp *Eco*147I/*Aat*II genomic fragment (bp 108026 to 104386 of BAC T6G21) used to complement the *pnt1-1* mutation. *PNT1* exons are represented by thick lines. The position of the cytosine-to-thymine change at bp 838 of the *PNT1* coding sequence in *pnt1-1* is noted. This nucleotide change results in a translational stop at codon 280. The position of the T-DNA insertion in SALK 069393 at bp 1051 of the *PNT1* coding sequence is also noted. The full-length *PNT1* cDNA sequence is available from GenBank/EMBL/DDBJ under accession number BX831719.

(B) Expression analysis of *PNT1* in different tissue types. *PNT1* is expressed at low levels in 7-d-old seedling roots, 7-d-old seedling hypocotyls and cotyledons, 4-week-old leaves, and 4-week-old inflorescence stems and at higher levels in flowers and inflorescences from 4-week-old plants. rRNA stained with methylene blue is shown as a loading control.

(C) The predicted PNT1 protein is 38% identical to human PIG-M. Alignment of PNT1 and PIG-M predicted protein sequences. Identical residues are boxed in black. The signature DxD glycosyltransferase motif is shown in brackets (Maeda et al., 2001). The position of the stop codon in *pnt1-1* is marked with an asterisk, and the position of the T-DNA insertion in *pnt1-2* is marked with a triangle.

treatment with phospholipase C (Sedbrook et al., 2002). Figure 7A shows the results of protein gel blot detection of SKU5 protein from wild-type, *pnt1*, *pnt2*, *pnt3*, *pnt4*, and *pnt5* embryo extracts. SKU5 protein was present in wild-type embryos but undetectable in *pnt1-pnt4*. Two faint bands of slightly lower molecular weight are visible on the *pnt5* blot, suggesting that *pnt5-1* is a leaky allele or that loss of the *PNT5* gene product does not lead to the degradation of all detectable SKU5 protein. Similar to embryos, SKU5 is abundant in wild-type callus but undetectable in *pnt1* callus (Figure 7A). Figure 7B shows the detection of PMR6 and COBRA protein from extracts of wild-type and *pnt1* callus. Based on the presence of GPI-anchoring sequence motifs, both PMR6 and COB have been proposed to be GPI anchored (Schindelman et al., 2001; Vogel et al., 2002). PMR6 protein is abundant in wild-type extracts and undetectable in *pnt1* extracts, whereas COB is present in the wild type and strongly reduced in *pnt1* extracts.

The high sequence identity of PNT1 and PIG-M and the demonstration that the GAP SKU5 is absent in *pnt1* embryos provide strong evidence that PNT1 functions as the first mannosyltransferase in GPI anchor biosynthesis in Arabidopsis. The absence or strong decrease of SKU5 in the other four *pnt* mutants suggests that they have biochemical defects related to that in *pnt1*, and it seems likely that they encode other functions in the pathway for GPI anchor biosynthesis.

DISCUSSION

Functional evidence for the role of GAPs in plant physiology and development is largely lacking (Borner et al., 2003). In this work, analysis of mutations in the Arabidopsis *PNT* genes demonstrates the importance of GAPs in cell wall synthesis and development. Surprisingly, the extreme defects in cell wall ultrastructure seen in *pnt1* embryos were not seen in callus tissue generated from *pnt1* embryos. This result suggests that GAPs play a more important role in cell wall synthesis during coordinated multicellular growth than in proliferation of undifferentiated tissue, such as callus.

pnt Mutants Lack GAPs

The enzymatic steps involved in production of the GPI anchor are represented in schematic form in Figure 8. Although some details

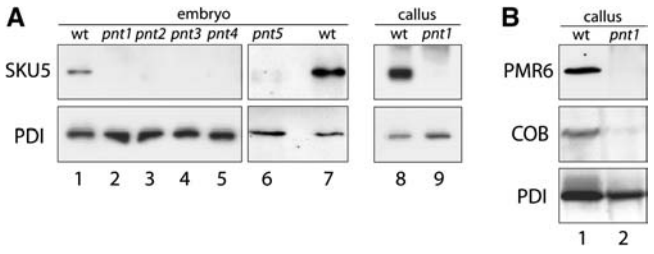

Figure 7. Absence of GAPs in *pnt* Mutants.

(A) Protein gel blot detection of SKU5 and protein disulfide isomerase from extracts of wild-type and *pnt1*, *pnt2*, *pnt3*, *pnt4*, and *pnt5* embryos and from wild-type and *pnt1* callus tissue. Protein disulfide isomerase (PDI) is shown as a loading control.

(B) Protein gel blot detection of PMR6, COB, and protein disulfide isomerase from wild-type and *pnt1* callus extracts. Protein disulfide isomerase (PDI) is shown as a loading control.

vary among animals, yeast, trypanosomes, and plants, synthesis of the core structure is essentially conserved. In mammalian cells, loss of any of the functions required for making the GPI anchor results in termination of anchor synthesis (reviewed in Kinoshita and Inoue, 2000). Furthermore, lack of transfer of the membrane-associated protein precursor to a functional GPI anchor results in ER retention and degradation of the untransferred protein (Field et al., 1994). This degradation can be accomplished via a pathway specific for ER-localized proteins (reviewed in Bonifacio and Lippincott-Schwartz, 1991). Using antibodies to the Arabidopsis GAP SKU5 (Sedbrook et al., 2002) and to the predicted GAPs COBRA and PMR6 (Schindelman et al., 2001; Vogel et al., 2002), we have shown that these proteins are diminished or undetectable in *pnt1* embryos and callus. We propose that the loss of the GAPs SKU5, COB, and PMR6 in *pnt1* is due to degradation of these proteins in the absence of their transfer to a functional GPI anchor (hatched box, Figure 8). In view of the effect of the *pnt1* mutation on these three proteins, it is likely that the lack of GPI mannosyltransferase I activity in *pnt1* mutants affects the targeting and stability of most or all GPI-anchored proteins.

The phenotype of *pnt1* embryos demonstrates that GAPs are required for cell wall biosynthesis and proper development of the shoot and root meristem during embryogenesis. Lalanne et al. (2004) have also recently described mutants of Arabidopsis with defects in GPI anchoring. The *seth1* and *seth2* mutants were recovered as male sterile plants in which pollen tube growth is defective. *SETH1* corresponds to PIG-C, phosphatidylinositol glucan synthase subunit C, and *SETH2* corresponds to PIG-A, GPI-*N*-acetylglucosaminyltransferase. Both proteins are part of the GPI-*N*-acetylglucosaminyltransferase enzyme complex that is required for addition of GlcNAc to the phosphatidylinositol membrane anchor, the first step in GPI anchor biosynthesis (step

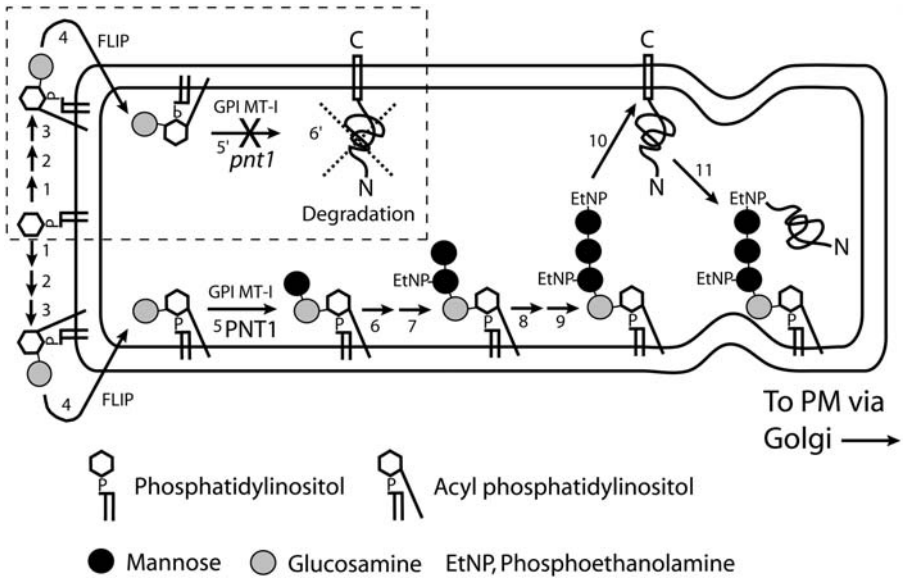

Figure 8. Synthesis of the GPI Anchor and Transfer of the Anchor to Proteins in Wild-Type and *pnt1* Cells.

For simplicity, some intermediates are not shown. Enzymatic steps are as follows: 1, generation of GlcNAc-PI from UDP-GlcNAc and phosphatidylinositol; 2, deacetylation of GlcNAc-PI to GlcN-PI; 3, acylation of GlcN-PI; 4, GlcN-acyl-PI is flipped from cytosolic to lumenal side of ER; 5, first mannose transferred to GlcN-acyl-PI by PIG-M enzyme; 6, phosphoethanolamine side chain added to Man-GlcN-acyl-PI; 7 and 8, second and third mannoses added to EtNP-Man-GlcN-acyl-PI; 9, EtNP added to third mannose of Man-Man-(EtNP)Man-GlcN-acyl-PI; 10, transamidation transfer of C-terminal membrane bound protein precursor to GPI anchor; 11, secretion of GAP (by way of Golgi) to plasma membrane. Hatched box: proposed GPI anchor synthesis pathway in *pnt1* cells (steps 1 to 6′). In the *pnt1* mutant, steps 1 to 4 occur as in wild-type cells, but in the absence of PNT1 function, the first mannose is not added to GlcN-acyl-PI, and GPI-anchor biosynthesis is arrested (step 5′). In the absence of a complete GPI anchor, the C-terminal membrane-bound protein precursor cannot be transferred to a GPI anchor and is eventually degraded (step 6′). Figure modified from Kinoshita and Inoue (2000).

1 in Figure 8; Kinoshita and Inoue, 2000). Thus, both *SETH* genes act at an earlier step in GPI anchor biosynthesis than *PNT1*. Because the *seth* mutants are essentially completely male sterile, the phenotype of homozygous embryos was not investigated by Lalanne et al. (2004). We expect that homozygous *seth* embryos would have the same phenotype as the *pnt* mutants.

That the *pnt1-1* allele is transmitted through the pollen (albeit at a low frequency) may indicate that this allele encodes some residual GPI-mannosyltransferase I activity. In support of this hypothesis, the stop codon in the *pnt1-1* allele occurs after the signature DxD glycosyltransferase motif shown by Maeda et al. (2001) to be essential for PIG-M enzyme activity, and we detected a low amount of COB protein in *pnt1* embryos. Analysis of *pnt1-2*, a T-DNA–induced allele of *PNT1*, did not help to resolve this issue because the T-DNA insertion in *pnt1-2* occurs near the C terminus of the protein, downstream of the stop codon in *pnt1-1* and further downstream of the DxD glycosyltransferase motif. Indeed, the *pnt1-2* allele was seen to have a weaker pollen transmission defect than the *pnt1-1* allele.

Importance of GAPs for Cell Wall Biosynthesis

pnt1 embryos have a significant decrease in crystalline cellulose, coupled with increases in cell wall neutral sugars and pectin. Furthermore, *pnt1* embryos also show considerable amounts of ectopic deposition of cell wall components, including callose. How can these observations be interpreted? It is likely that the effect on the cell wall of loss of *PNT1* function is indirect: the cell wall phenotypes of *pnt1* embryos are the result of the absence of GAPs that are required for cell wall synthesis and assembly. Recent mutational analysis of a small number of GAPs, the prediction of the total set of GAPs in Arabidopsis, and some inhibitor studies allow the identification of candidate proteins and processes responsible for the cell wall defects observed in *pnt1* embryos.

Conditional mutations in the *COB* gene result in a decrease in crystalline cellulose of ~30% in seedling roots (Schindelman et al., 2001). The *BC1* gene of rice is a homolog of *COB*, and *bc1* plants have a 30% reduction in crystalline cellulose in vascular bundles and ground tissue (Li et al., 2003). Although the biochemical role of COB in cellulose synthesis is unknown, this genetic evidence demonstrates that *COB*-like genes are required for normal levels of cellulose. We found that COB was undetectable in embryo extracts but present in callus tissue, where levels of COB protein are strongly reduced in *pnt1* compared with the wild type. *COB* is one of an 11-member gene family, several of which are expressed during embryogenesis, and all of which have been either predicted or shown to be GPI anchored (Roudier et al., 2002; Borner et al., 2003). The magnitude of cellulose decrease in cob roots (~30%) is similar to that seen in *pnt1* embryos (40%). Thus, a likely explanation for the cellulose decrease seen in *pnt1* embryos is that lack of a functional GPI anchor in *pnt1* mutants leads to degradation or mislocalization of the COB family members that are normally required for cellulose synthesis or deposition during embryogenesis.

Genetic and inhibitor studies also point to an important role for AGPs in cell expansion and cell wall assembly. AGPs are extracellular proteoglycans that are often expressed in a cell- or tissue-specific manner (Maewska-Sawka and Nothnagel, 2000). All 16 classical AGPs of Arabidopsis are predicted to be GPI anchored (Schultz et al., 2000). Growth of Arabidopsis seedlings on Yariv reagent, a synthetic phenyl glycoside that binds AGPs, resulted in seedlings with short, swollen roots (Willats and Knox, 1996). In addition, the *root epidermal bulger1* mutant of Arabidopsis has decreased amounts of AGPs in the root epidermal cells (Ding and Zhu, 1997; Seifert et al., 2002). Loss of SOS5, a plasma membrane–localized protein with AGP and fasciclin domains that is predicted to be GPI anchored, results in seedlings with swollen root tips when grown under salt stress conditions. Cell walls of the *sos5* mutant have decreased electron-dense staining in transmission electron micrographs, characteristic of decreased amounts of pectin (Shi et al., 2003).

Perhaps the strongest evidence for the role of AGPs in contributing to cell wall structure comes from a study by Roy et al. (1998), where lily (*Lilium longiflorum*) pollen tubes were grown in the presence of Yariv reagent. Ultrastructural examination of treated pollen tubes revealed that Yariv reagent interfered with cell wall assembly; secretory vesicles released their contents into the periplasmic space, but these vesicle contents, primarily pectin and callose, the main carbohydrates of pollen walls, were not integrated into the cell wall in a normal manner. Instead, large amounts of these materials accumulated randomly in the extracellular space, in a manner strikingly similar to what has been observed in *pnt1* embryos. Roles for AGPs in chaperoning cell wall polymers through the secretory pathway and in integrating these polymers into the cell wall have previously been proposed (Gibeaut and Carpita, 1994; Kieliszewski and Lamport, 1994). Thus, the abnormal deposition of pectin and xyloglucans in *pnt1* mutants might be due to the absence of AGPs. This could also explain the increased amounts of cell wall material deposited in *pnt1* embryos: a lack of properly integrated pectins and xyloglucans might prompt the cells to attempt to compensate for this deficiency by increasing the synthesis and export of these polymers.

Ectopic callose deposition is characteristic of the *pnt1* phenotype. Large amounts of ectopic callose production during embryogenesis were previously observed in the *cyt1* mutant, which shares several phenotypic aspects with *pnt1*, including reduced crystalline cellulose and abnormal accumulation of cell wall material (Nickle and Meinke, 1998; Lukowitz et al., 2001). This phenotypic similarity is not a coincidence because the *CYT1* gene encodes an enzyme that is required for the production of GDP-mannose, an essential component of the core GPI anchor as well as the core *N*-glycan (Lukowitz et al., 2001). *pnt1* and *cyt1* embryos are unique among cell wall mutants of plants in the extent of their uncontrolled deposition of xyloglucans and pectins into the extracellular space. This uncontrolled wall deposition, coupled with a decrease in cellulose, likely compromises the mechanical integrity of the wall and could therefore trigger callose synthesis as part of a stress or wound response. A second, nonexclusive explanation for the accumulation of callose in the mutants is suggested by the experiments showing that treatment of Arabidopsis cell cultures with Yariv reagent induces callose production and programmed cell death (Gao and Showalter, 1999; Guan and Nothnagel, 2004). These experiments

with Yariv reagent also suggest that a lack of AGPs in *pnt1* embryos and cells might be responsible for the seedling lethality of *pnt1* and necrosis seen in *pnt1* callus. It is intriguing that callus grown from *pnt1* embryos lacks the massive ectopic deposition of cell wall material seen in *pnt1* embryos. This suggests that there is a fundamental difference in the importance of GAPs to cell wall synthesis in embryos and callus. The difference might arise because of a different composition of the structural components of the cell wall in callus cells, as suggested by analysis of sugar composition of different tissues of Arabidopsis (Richmond and Somerville, 2001).

As in Arabidopsis, GPI anchor synthesis mutants in yeast are lethal (Leidich et al., 1994). Yeast GAPs are required for maintaining the architecture of the yeast cell wall, and the GPI anchor itself is often incorporated along with the GAP as a structural component of the wall (Kapteyn et al., 1999). Our analysis of *pnt1* embryos shows that in plants, like in yeast, GAPs play an important role in organizing cell wall structure. However, only a subset of the GAPs of Arabidopsis are predicted to be involved in cell wall synthesis or assembly (Borner et al., 2003). Many of the remaining GAPs of Arabidopsis likely play essential roles in cell–cell signaling and multicellular development.

METHODS

Plant Material, Growth Conditions, and Genetic Mapping

All mutant lines, isolated in the genetic screens described by Gillmor et al. (2002), were generated in the Landsberg *erecta* ecotype. The *pnt1-1* line P13 (ABRC stock number CS6120) and *pnt2-1* line 2-1 (ABRC stock number CS6121) were generated by ethyl methanesulfonate mutagenesis. The *pnt2-2* line FN70, the *pnt3-1* line FN45 (ABRC stock number CS6122), the *pnt4-1* line FN72 (ABRC stock number CS6123), and the *pnt5-1* line FN105 were generated by fast neutron mutagenesis. SALK_069393 containing the T-DNA allele *pnt1-2* in the Columbia ecotype was obtained from the ABRC. Mutant lines are available from the ABRC through The Arabidopsis Information Resource at www.arabidopsis.org. Plants in soil and seedlings on tissue culture plates were grown as described by Gillmor et al. (2002). Callus was produced from wild-type and *pnt1* embryos dissected from seed coats at the late bent cotyledon stage, while the embryos were still green, and grown on media described by Encina et al. (2001). Mapping of *PNT* genes was performed as described by Lukowitz et al. (2000). Primer sequences for all PCR-based genetic markers are available from The Arabidopsis Information Resource at www.arabidopsis.org.

Confocal, Light, and Electron Microscopy

Preparation of embryos for confocal and electron microscopy, collection of data, and processing of data were performed as described by Gillmor et al. (2002). For fluorescent immunostaining of embryo sections, osmium tetroxide–stained semithin sections were first etched in 0.5% H_2O_2 for 10 min, followed by two rinses with distilled water for 5 min, then 100 mM HCl for 10 min, followed by two rinses with distilled water for 5 min. Staining with CCRC M1, JIM5, and anti-β-1,3 glucan (Biosupplies, Parkville, Australia) monoclonal antibodies was then performed as described by Rhee and Somerville (1998). Callose staining with sirofluor was performed as described by Lukowitz et al. (2001). Fluorescence and immunofluorescence embryo images were acquired with a Leica DMRB compound microscope (Wetzlar, Germany) with 20× air and 100× oil objectives using a SPOT camera (Diagnostic Instruments, Sterling Heights, MI). Immunofluorescence images of callose were aquired with a Nikon Eclipse E600 microscope (Tokyo, Japan) at 40× magnification using a Spot RT Slider camera (Diagnostic Instruments). Confocal images of embryos were obtained with a Bio-Rad MRC 1024 confocal system (Hercules, CA) with a Nikon microscope using 20× and 40× air objectives. Light and confocal microscopy were performed at room temperature (~22°C). Transmission electron microscopy images were obtained with Philips 410 (Eindhoven, The Netherlands) and Jeol 1230 transmission electron microscopes (Peabody, MA).

Molecular Biology

The *PNT1* gene (At5g22130) was sequenced directly from gel-purified PCR products amplified from genomic DNA prepared from wild-type and *pnt1-1* embryos, using an ABI 310 sequencer (Perkin-Elmer Applied Biosystems, Foster City, CA). For complementation of the *pnt1* phenotype, a 3641-bp *Eco*147I/*Aat*II genomic fragment was excised from BAC T6G21 (obtained from the ABRC) and subcloned into the pCAMBIA 3300 binary vector, modified to contain *Eco*147I and *Aat*II sites, to produce plasmid pCS702. Plasmid pCS702 was then transformed into *Agrobacterium tumefaciens* and used to transform a mixed population of *pnt1*/*PNT1* and *PNT1*/*PNT1* plants. *pnt1*/*pnt1* homozygous plants were identified in the T1 generation, indicating complementation of the *pnt1* mutation. RNA gel blot analysis of *PNT1* gene expression was performed according to standard protocols using the full-length *PNT1* cDNA labeled with ^{32}P and total RNA extracted with Trizol reagent (Sigma-Aldrich, St. Louis, MO).

Protein Gel Blot Analysis

Wild-type and *pnt* embryo and callus tissue were ground in a micro mortar and pestle in 50 μL of grinding buffer (50 mM sodium phosphate buffer, pH 8.0, and 300 mM NaCl) plus 1× Calbiochem protease inhibitor cocktail set I (San Diego, CA). Proteins were quantified using a Bradford protein assay kit (Bio-Rad). Ten micrograms of total protein extract was loaded per lane, separated by 10% SDS-PAGE, and electroblotted using semi-dry transfer to polyvinylidene difluoride membrane. SKU5 primary antibody was used at a dilution of 1:1000, protein disulfide isomerase antibody (http://rosebiotech.com/) was used at a dilution of 1:2500, COB antibody used at a dilution of 1:3000, and PMR6 antibody used at a dilution of 1:3000. Primary antibodies were visualized by incubation with goat anti-rabbit IgG secondary antibodies conjugated to horseradish peroxidase (Bio-Rad) followed by a chemiluminescence reaction (SuperSignal; Pierce Chemical, Rockford, IL).

Cell Wall Analysis

Cell wall analysis of wild-type and *pnt1* embryos was performed as described by Gillmor et al. (2002).

ACKNOWLEDGMENTS

The expert technical assistance of R. Gillmor (Carnegie Institution, Stanford, CA) is gratefully acknowledged. Thanks to F. Roudier and P. Benfey (Duke University, Durham, NC) for the kind gift of COBRA antibody, to J. Vogel (USDA, Albany, CA) and S. Somerville (Carnegie Institution) for the PMR6 antibody, to P. Knox (Leeds University, Leeds, UK) for the JIM5 antibody, and to M. Hahn (University of Georgia, Athens, GA) for the CCRC M1 antibody. Thanks to B. Fang and A. Paredez for genetic mapping, to H. Youngs for advice on cell wall chemistry, and to Genoscope (INRA, Evry, France) for the full-length *PNT1* cDNA. C.S.G. was supported by a U.S. Department of Energy/National Science Foundation/USDA triagency training grant and by

a grant from the U.S. Department of Energy (DE-FG02-03ER20133). W.L. was supported by a fellowship from the Human Frontier Science Program, a Barbara McClintock fellowship from the Carnegie Institution, and by USDA Grant CSREES 00-35304-9394. J.C.S. was supported by a National Institutes of Health postdoctoral fellowship.

Received February 13, 2005; accepted February 18, 2005.

REFERENCES

Acosta-García, G., and Vielle-Calzada, J.-P. (2004). A classical arabinogalactan protein is essential for the initiation of female gametogenesis in Arabidopsis. Plant Cell **16,** 2614–2628.

Beeckman, T., Przemeck, G.H.K., Stamatiou, G., Lau, R., Terryn, N., De Rycke, R., Inzé, D., and Berleth, T. (2002). Genetic complexity of cellulose synthase A gene function in Arabidopsis embryogenesis. Plant Physiol. **130,** 1883–1893.

Bonifacio, J.S., and Lippincott-Schwartz, J. (1991). Degradation of proteins within the endoplasmic reticulum. Curr. Opin. Cell Biol. **3,** 592–600.

Borner, G.H., Lilley, K.S., Stephens, T.J., and Dupree, P. (2003). Identification of glycosylphosphatidylinositol-anchored proteins in Arabidopsis. A proteomic and genomic analysis. Plant Physiol. **132,** 568–577.

Borner, G.H., Sherrier, D.J., Stevens, T.J., Arkin, I.T., and Dupree, P. (2002). Prediction of glycosylphosphatidylinositol-anchored proteins in Arabidopsis. A genomic analysis. Plant Physiol. **129,** 486–499.

Borner, G.H., Sherrier, D.J., Weimar, T., Michaelson, L.V., Hawkins, N.D., Macaskill, A., Napier, J.A., Beale, M.H., Lilley, K.S., and Dupree, P. (2005). Analysis of detergent-resistant membranes in Arabidopsis. Evidence for plasma membrane lipid rafts. Plant Physiol. **137,** 104–116.

Burn, J.E., Hurley, U.A., Birch, R.J., Arioli, T., Cork, A., and Williamson, R.E. (2002). The cellulose deficient Arabidopsis mutant *rsw3* is defective in a gene encoding a putative glucosidase II, an enzyme processing N-glycans during ER quality control. Plant J. **32,** 949–960.

Caro, L.H.P., Tettelin, H., Vossen, J.H., Ram, A.F.J., Van Den Ende, H., and Klis, F.M. (1997). *In silico* identification of glycosylphosphatidylinositol-anchored plasma-membrane and cell wall proteins of *Saccharomyces cerevisiae*. Yeast **13,** 1477–1489.

Delmer, D. (1987). Cellulose biosynthesis. Annu. Rev. Plant Physiol. **38,** 259–290.

Ding, L., and Zhu, J.-K. (1997). A role for arabinogalactan-proteins in root epidermal cell expansion. Planta **203,** 289–294.

Eisenhaber, B., Wildpaner, M., Schultz, C.J., Borner, G.H., Dupree, P., and Eisenhaber, F. (2003). Glycosylphosphatidylinositol lipid anchoring of plant proteins. Sensitive prediction from sequence- and genome-wide studies for Arabidopsis and rice. Plant Physiol. **133,** 1691–1701.

Encina, C.L., Constantin, M., and Botella, J. (2001). An easy and reliable method for establishment and maintenance of leaf and root cell cultures of *Arabidopsis thaliana*. Plant Mol. Biol. Report. **19,** 245–248.

Ferguson, M.A.J. (1999). The structure, biosynthesis and functions of glycosylphosphatidylinositol anchors, and the contributions of trypanosome research. J. Cell Sci. **112,** 2799–2809.

Field, M.C., Moran, P., Li, W., Keller, G.-A., and Caras, I.W. (1994). Retention and degradation of proteins containing an uncleaved glycosylphosphatidylinositol signal. J. Biol. Chem. **269,** 10830–10837.

Gao, M., and Showalter, A.M. (1999). Yariv reagent treatment incudes programmed cell death in Arabidopsis cell cultures and implicates arabinogalactan protein involvement. Plant J. **19,** 321–331.

Gaspar, Y., Johnson, K.L., McKenna, J.A., Bacic, A., and Schulz, C.J. (2001). The complex structures of arabinogalactan-proteins and the journey towards understanding function. Plant Mol. Biol. **47,** 161–176.

Gibeaut, D.M., and Carpita, N.C. (1994). Biosynthesis of plant cell wall polysaccharides. FASEB J. **8,** 904–915.

Gillmor, C.S., Poindexter, P., Lorieau, J., Palcic, M.M., and Somerville, C. (2002). α-Glucosidase I is required for cellulose biosynthesis and morphogenesis in Arabidopsis. J. Cell Biol. **156,** 1003–1013.

Guan, Y., and Nothnagel, E.A. (2004). Binding of arabinogalactan proteins by Yariv phenylglycoside triggers wound-like responses in Arabidopsis cell cultures. Plant Physiol. **135,** 1346–1366.

Jürgens, G., and Mayer, U. (1994). *Arabidopsis*. In Embryos: Color Atlas of Development, J.B.L. Bard, ed (London: Wolfe), pp. 7–21.

Kapteyn, J.C., Van Den Ende, H., and Klis, F.M. (1999). The contribution of cell wall proteins to the organization of the yeast cell wall. Biochim. Biophys. Acta **1426,** 373–383.

Kieliszewski, M.J., and Lamport, D.T.A. (1994). Extensin: Repetitive motifs, functional sites, post-translational codes, and phylogeny. Plant J. **5,** 157–172.

Kinoshita, T., and Inoue, N. (2000). Dissecting and manipulating the pathway for glycosylphosphatidylinositol-anchor biosynthesis. Curr. Opin. Chem. Biol. **4,** 632–638.

Knox, J.P., Linstead, P.J., King, J., Cooper, C., and Roberts, K. (1990). Pectin esterification is spatially regulated both within cell walls and between developing tissues of root apices. Planta **181,** 512–521.

Lalanne, E., Honys, D., Johnson, A., Borner, G.H.H., Lilley, K.S., Dupree, P., Grossniklaus, U., and Twell, D. (2004). *SETH1* and *SETH2*, two components of the glycosylphosphatidylinositol anchor biosynthetic pathway, are required for pollen germination and tube growth in Arabidopsis. Plant Cell **16,** 229–240.

Leidich, S.D., Drapp, D.A., and Orlean, P. (1994). A conditionally lethal yeast mutant blocked at the first step in glycosyl phosphatidylinositol anchor synthesis. J. Biol. Chem. **269,** 10193–10196.

Li, Y., Qian, Q., Zhou, Y., Yan, M., Sun, L., Zhang, M., Fu, Z., Wang, Y., Han, B., Pang, X., Chen, M., and Li, J. (2003). *BRITTLE CULM1*, which encodes a COBRA-like protein, affects the mechanical properties of rice plants. Plant Cell **15,** 2020–2031.

Lukowitz, W., Gillmor, C.S., and Scheible, W.-R. (2000). Positional cloning in Arabidopsis. Why it feels good to have a genome initiative working for you. Plant Physiol. **123,** 795–805.

Lukowitz, W., Nickle, T.C., Meinke, D.W., Last, R.L., Conklin, P.L., and Somerville, C.R. (2001). Arabidopsis *cyt1* mutants are deficient in a mannose-1-phosphate guanylyltransferase and point to a requirement of N-linked glycosylation for cellulose biosynthesis. Proc. Natl. Acad. Sci. USA **98,** 2262–2267.

Maeda, Y., Watanabe, R., Harris, C.L., Hong, Y., Ohishi, K., Kinoshita, K., and Kinoshita, T. (2001). PIG-M transfers the first mannose to glycosylphosphatidylinositol on the lumenal side of the ER. EMBO J. **20,** 250–261.

Maewska-Sawka, A., and Nothnagel, E.A. (2000). The multiple roles of arabinogalactan proteins in plant development. Plant Physiol. **122,** 3–9.

Nickle, T.C., and Meinke, D.W. (1998). A cytokinesis-defective mutant of Arabidopsis (*cyt1*) characterized by embryonic lethality, incomplete cell walls, and excessive callose accumulation. Plant J. **15,** 321–332.

Peskan, T., Westermann, M., and Oelmüller, R. (2000). Identification of low-density Triton X-100-insoluble plasma membrane microdomains in higher plants. Eur. J. Biochem. **267,** 6989–6995.

Puhlmann, J., Bucheli, E., Swain, M.J., Dunning, N., Albersheim, P., Darvill, A.G., and Hahn, M.G. (1994). Generation of monoclonal antibodies against plant cell-wall polysaccharides. I. Characterization

of a monclonal antibody to a terminal α-(1–>2)-linked fucosyl-containing epitope. Plant Physiol. **104,** 699–710.

Rhee, S.Y., and Somerville, C.R. (1998). Tetrad pollen formation in quartet mutants of *Arabidopsis thaliana* is associated with persistence of pectic polysaccharides of the pollen mother cell wall. Plant J. **15,** 79–88.

Richmond, T., and Somerville, C.R. (2001). Integrative approaches to determining Csl function. Plant Mol. Biol. **47,** 131–143.

Roudier, F., Schindelman, G., DeSalle, R., and Benfey, P.N. (2002). The COBRA family of putative GPI-anchored proteins in Arabidopsis: A new fellowship in expansion. Plant Physiol. **130,** 538–548.

Roy, S., Jauh, G.Y., Hepler, P.K., and Lord, E.M. (1998). Effects of Yariv phenylglycoside on cell wall assembly in the lily pollen tube. Planta **204,** 450–458.

Schindelman, G., Morikami, A., Jung, J., Baskin, T.I., Carpita, N.C., Derbyshire, P., McCann, M.C., and Benfey, P.N. (2001). *COBRA* encodes a putative GPI-anchored protein, which is polarly localized and necessary for oriented cell expansion in Arabidopsis. Genes Dev. **15,** 1115–1127.

Schultz, C.J., Johnson, K.L., Currie, G., and Bacic, A. (2000). The classical arabinogalactan protein gene family of Arabidopsis. Plant Cell **12,** 1751–1767.

Sedbrook, J.C., Carroll, K.L., Hung, K.F., Masson, P.H., and Somerville, C.R. (2002). The Arabidopsis *SKU5* gene encodes an extracellular glycosyl phosphatidylinositol-anchored glycoprotein involved in directional root growth. Plant Cell **14,** 1635–1648.

Seifert, G.J., Barber, C., Wells, B., Dolan, L., and Roberts, K. (2002). Galactose biosynthesis in Arabidopsis: Genetic evidence for substrate channeling from UDP-D-Galactose into cell wall polymers. Curr. Biol. **12,** 1840–1845.

Selleck, S.B. (2000). Proteoglycans and pattern formation. Sugar biochemistry meets developmental genetics. Trends Genet. **16,** 206–212.

Shi, H., Kim, Y.-S., Guo, Y., Stevenson, B., and Zhu, J.-K. (2003). The Arabidopsis *SOS5* locus encodes a putative cell surface adhesion protein and is required for normal cell expansion. Plant Cell **15,** 19–32.

Stone, B.A., Evans, N.A., Bonig, I., and Clarke, A.E. (1984). The application of Sirofluor, a chemically defined fluorochrome from analine blue for the histochemical detection of callose. Protoplasma **122,** 191–195.

Sun, W., Kieliszewski, M.J., and Showalter, A.M. (2004a). Overexpression of tomato LeAGP-1 arabinogalactan-protein promotes lateral branching and hampers reproductive development. Plant J. **40,** 870–881.

Sun, W., Zhao, Z.D., Hare, M.C., Kieliszewski, M.J., and Showalter, A.M. (2004b). Tomato LeAGP-1 is a plasma membrane-bound, glycosylphosphatidylinositol-anhored arabinogalactan-protein. Physiol. Plant. **120,** 319–327.

Torres-Ruíz, R.A., and Jürgens, G. (1994). Mutations in the *FASS* gene uncouple pattern formation and morphogenesis in Arabidopsis development. Development **120,** 2967–2978.

Vogel, J.P., Raab, T.K., Schiff, C., and Somerville, S.C. (2002). *PMR6*, a pectate lyase-like gene required for powdery mildew susceptibility in Arabidopsis. Plant Cell **14,** 2095–2106.

Willats, W.G.T., and Knox, J.P. (1996). A role for arabinogalactan-proteins in plant cell expansion: Evidence from studies on the interaction of B-glucosyl Yariv reagent with seedlings of *Arabidopsis thaliana*. Plant J. **9,** 919–925.

Williamson, R.E., Burn, J.E., and Hocart, C.H. (2002). Towards the mechanism of cellulose synthesis. Trends Plant Sci. **7,** 461–467.

Youl, J.J., Bacic, A., and Oxley, D. (1998). Arabinogalactan-proteins from *Nicotiana alata* and *Pyrus communis* contain glycosylphosphatidylinositol membrane anchors. Proc. Natl. Acad. Sci. USA **95,** 7921–7926.